electronics

MDPI

Article

A Vibration Fault Signal Identification Method via SEST

Xuemei Li [1,2], Chunyang Wang [1,3,*], Xuelian Liu [3], Bo Xiao [4] and Zishuo Wang [1]

[1] School of Electronic and Information Engineering, Changchun University of Science and Technology, Changchun 130022, China; lixuemei556677@163.com (X.L.); wangzishuo20@163.com (Z.W.)
[2] School of Mechanical and Control Engineering, Baicheng Normal University, Baicheng 137000, China
[3] Xi'an Key Laboratory of Active Photoelectric Imaging Detection Technology, Xi'an Technological University, Xi'an 710021, China; liuxuelian@xatu.edu.cn
[4] School of Optoelectronic Engineering, Xi'an Technological University, Xi'an 710021, China; xiaobo@xatu.edu.cn
* Correspondence: wangchunyang19@163.com; Tel.: +86-13578898897

Abstract: (1) Background: with the development of intelligent transportation, effectively collecting and identifying the working state of vehicles is conducive to the analysis and processing of vehicle information by internet of vehicles, so as to reduce the occurrence of traffic accidents. Aiming at the problem of low identification accuracy of the mechanical vibration fault signal, a signal identification method based on time-frequency detection is introduced; (2) Methods: this paper constructs a parameter model of the synchroextracting S transform on the basis of the poor time-frequency concentration of the original S transform; (3) Results: in the case of SNR = −5~+30 dB, compared with other transformations, the Rényi entropy value of *SEST* is the smallest, and the Rényi entropy value is 0.5246 when SNR = +22 dB; (4) Conclusions: through simulation comparison and analysis, the excellent time-frequency concentration and anti-noise characteristics of the *SEST* are highlighted, and the rotor vibration fault signals such as rotor misalignment, unbalance and bearing wear are identified by *SEST*.

Keywords: synchroextracting S transform; signal identification; time-frequency concentration; vibration fault

Citation: Li, X.; Wang, C.; Liu, X.; Xiao, B.; Wang, Z. A Vibration Fault Signal Identification Method via SEST. *Electronics* **2022**, *11*, 1300. https://doi.org/10.3390/electronics11091300

Academic Editors: Zhiwei Zhao, Jorge Ortiz and Guohao Lan

Received: 6 March 2022
Accepted: 18 April 2022
Published: 20 April 2022

1. Introduction

Mechanical vibration faults are mainly caused by the vibration of components due to mechanical or electromagnetic factors. It is common in industrial and agricultural machinery, transportation tools and other equipment [1,2]. With the advent of the era of intelligent transportation, how to efficiently and quickly ensure the safe travel of vehicles under the background of internet of vehicles is a problem worth pondering. The real-time diagnosis and identification of vehicle faults, combined with the intelligent on-board system, can effectively extract the static and dynamic fault information of vehicles, which is conducive to the real-time supervision of vehicles and the intelligent production of vehicles, and can provide a guarantee for the implementation of intelligent transportation.

The vibration fault signal is composed of multiple instantaneous non-stationary vibration components, and how to accurately describe the local information of the signal and effectively extract the signal features are the keys to fault identification [3]. With regard to the diagnosis and identification analysis of vibration fault signals, two kinds of analysis methods are usually adopted. One is time-frequency analysis [4–6], such as when the short-time Fourier transform (*STFT*), fast Fourier transform (*FFT*), wavelet transform (*WT*), Hilbert–Huang transform (*HHT*) and Wigner–Ville distribution (*WVD*) take form in the original or various improved transforms. When the window width of the *STFT* is fixed, the time resolution and frequency resolution are mutually restricted and cannot simultaneously reach the optimum, and the time-frequency concentration is not dense. However, there is no cross-term interference [7]. Reference [8] proposed an analytical method for

aircraft vibration fault signals based on the *STFT*. By analyzing various influencing factors, including engine operation, external aerodynamic excitation, equipment operation and electrical interference, the time-frequency characteristics of flight vibration signals can be effectively obtained. In terms of algorithm improvement, reference [9] combined empirical mode decomposition (*EMD*) with the *STFT* to address selecting a multi-component signal window function and window width. *EMD* is used to carry out the adaptive decomposition of cylinder head vibration signals, and then the *STFT* is performed by selectively targeting the window function. The optimal *STFT* time-frequency distribution of the original signal is obtained by linear superposition, on the basis of which the time-frequency resolution of the *STFT* is effectively advanced. The spectrum leakage and fence effect of *FFT* damping characteristics and local characteristics cannot be analyzed. To facilitate algorithm improvement [10,11], reference [12] proposed a characteristic extraction method for rotor vibration signal characteristics based on the *FFT* and empirical wavelet transform (*EWT*), combining the rotor characteristic frequency with *EWT* modal components to form multi-dimensional characteristic vectors, and the rotor states were identified by the K-means clustering method. The *WT* has multi-resolution characteristics, can characterize the local details of the signal, and is sensitive to singularity. It also has the ability to quickly capture fault mutations and has no cross-term interference, but it has difficulty extracting the attenuation characteristics of the signal. *WVD* can extract the edge characteristics and instantaneous frequency of vibration signals well, but it cannot accurately demonstrate the multi-component signals due to the existence of cross-term interference. The *HHT* decomposes the vibration signal by *EMD*. Then, each decomposed intrinsic mode function (*IMF*) component is transformed by the Hilbert transform, and the instantaneous frequency and amplitude of the signal are obtained, thus fully characterizing the time-frequency distribution of the signal. However, the endpoint effect and mode aliasing effect of the *HHT* are highlighted. The original S transform (*ST*) is based on the *STFT* and *WT*, and exhibits the excellent characteristics of both; that is, it has variable multi-resolution and keeps the absolute phase of each component unchanged. It has strong sensitivity to the non-stationary characteristics of the signal transients, but the time-frequency concentration is not high. Since the window function of the *ST* is constant, it lacks adaptability to time-frequency characteristics. For this reason, the amplitude stretch factor and frequency-scale stretch factor of the window function are introduced to obtain the generalized S transform (*GST*). The *GST* can adaptively adjust window width with frequency change, but the non-optimal value of adjusting parameters has a great impact on the window function [13,14]. These time-frequency analysis methods complete fault diagnosis by extracting the characteristic information of the vibration fault signal. The application of this method does not need prior knowledge, but it cannot accurately represent the more complex time-frequency characteristics of non-stationary signals [15]. Additionally, the vibration fault signal is usually weak, and is easily concealed by noise or other feature information, which affects the identification of rotor faults [16]. G.Yu's two references have clearly shown that the time-frequency effect of the synchroextracting transform (*SET*) is better than that of the synchrosqueezing transform [17,18]. For *ST*, there is no need to compare and analyze the synchrosqueezing S transform and the synchroextracting S transform. Based on the *WT*, the synchrosqueezing wavelet transform (*SWT*) uses the synchrosqueezing method to redistribute the energy of the time-scale plane and "squeeze" the energy of the original time-frequency spectrum to the vicinity of the time-frequency ridge, which is not suitable for processing high-frequency signals [19,20].

As the non-parametric spectral estimation method, the most classic is the periodogram method. In 1967, Welch improved the periodogram method and proposed the Welch method, which uses smoothing and windowing measures to reduce the variance of frequency spectrum estimation, and has been effectively applied in practice [21]. With the development of modern spectrum estimation methods, Schmidt proposed multiple signal classification (*Music*) in 1986 [22–24] and Roy et al. proposed estimation of signal parameters by rotational invariance techniques (*ESPRIT*) in 1987 [25]. The minimum variance

spectrum estimation method, which was proposed by Capon in 1969, can adaptively construct filter banks through the observed signals to make the frequency signals of interest pass through without distortion, and can suppress the interference and noise of other frequency components to the greatest extent at the same time [26]. In 2009, Stoica et al. proposed an iterative adaptive approach (*IAA*) based on weighted least squares. Compared with Capon, *IAA* obtains higher resolution through cyclic iteration, and can process spectrum estimation in the case of uniform sampling and non-uniform sampling at the same time [27–29].

The other analysis method is intelligent identification; for example, back propagation neural network, deep belief network, convolutional neural network and other algorithms. Since the vibration fault of the motor rotor is unpredictable compared with intelligent identification methods, time-frequency analysis methods are more universal in the identification of vibration fault signals, and time-frequency concentration is often used as an evaluation index. Through the above analysis, in order to promote the signal extraction of tiny vibration faults in a motor rotor and meet the needs of multi-component processing without cross-term interference, energy attenuation or false information interference while achieving high time-frequency concentration, in this paper, based on the original *ST*, the *SET* is introduced to extract the time-frequency coefficients at the time-frequency ridge line of the original rotor vibration fault signal to obtain a new time-frequency spectrum with high concentration [30]. The combination of the original *ST* and *SET* is called the synchroextracting S transform (*SEST*). The time-frequency distribution of the *SEST* is presented as a clear straight line. Compared with the *STFT*, *GST*, *HHT*, *WT* and *ST*, the time-frequency concentration of the *SEST* is noticeably increased, the anti-noise effect is significant, and the rotor vibration fault signal can be clearly identified.

The rest of this paper is organized as follows. Section 2 focuses on the *SEST* method. Section 3 analyzes the performance of the *SEST* method for multi-component signal, evaluates the time-frequency concentration of the vibration fault signal by Rényi entropy, and compares it with other transform methods. The *SEST* method is applied to extract the characteristics of various rotor vibration fault signals in Section 4. Finally, conclusions are given in Section 5.

2. Synchroextracting S Transform Method

2.1. SEST Algorithm

To transform $x(t)$ by the *STFT*, its expression is as follows:

$$STFT_x(t,f) = \int_{-\infty}^{+\infty} x(\tau)m(\tau - t)e^{-j2\pi \cdot f \cdot \tau}d\tau \tag{1}$$

where $m(\tau - t)$ is the window function centered at time t, which determines the time-frequency resolution, and f is the frequency. From Equation (1), the window function $m(t)$ takes the normalized Gaussian window function, that is:

$$m(t) = \frac{|f|}{\sqrt{2\pi}}e^{-\frac{t^2 \cdot f^2}{2}} \tag{2}$$

The window width of the high-frequency band becomes narrower, and the time resolution increases in the time-frequency domain; the window width of the low-frequency band increases and the frequency resolution increases. As a result, the *ST* possesses the characteristics of multi-resolution and can improve the energy density in the time-frequency domain.

Equation (2) is substituted into Equation (1):

$$ST_x(t,f) = e^{-j2\pi \cdot f \cdot t}\frac{|f|}{\sqrt{2\pi}}\int_{-\infty}^{+\infty} x(\tau)e^{-\frac{(\tau-t)^2 \cdot f^2}{2}} \cdot e^{-j2\pi \cdot f \cdot (\tau - t)}d\tau \tag{3}$$

Let $w(\tau, f) = \frac{|f|}{\sqrt{2\pi}} e^{-\frac{f^2 \cdot \tau^2}{2}} \cdot e^{j2\pi \cdot f \cdot \tau}$; then, Equation (3) can be rewritten as follows:

$$ST_x(t, f) = e^{-j2\pi \cdot f \cdot t} \int_{-\infty}^{+\infty} x(\tau) \cdot (w(\tau - t, f))^* d\tau \tag{4}$$

where $(\cdot)^*$ is a conjugate operation.

Equation (4) is denoted in the form of a Fourier transform (*FT*), that is:

$$ST_x(t, f) = e^{-j2\pi \cdot f \cdot t} \int_{-\infty}^{+\infty} X(\xi) \cdot (W(\xi, f))^* \cdot e^{j2\pi \cdot \xi \cdot t} d\xi \tag{5}$$

where $X(\xi)$ is the *FT* of $x(t)$, $W(\cdot)$ is the *FT* of $w(\cdot)$, and ξ acts as the frequency.

For the convenience of analysis, a mathematical model of the harmonic signal is set as:

$$x(t) = A \cdot e^{j2\pi \cdot f_0 \cdot t} \tag{6}$$

where A is the amplitude and f_0 is the frequency.

The *FT* of $x(t)$ is:

$$X(\xi) = A \cdot \delta(\xi - f_0) \tag{7}$$

where ξ is the frequency and $\delta(\cdot)$ is the impulse function with its value as:

$$A \cdot \delta(\xi - f_0) = \begin{cases} A & \xi = f_0 \\ 0 & \xi \neq f_0 \end{cases} \tag{8}$$

Equation (7) is substituted into Equation (5), and we can obtain:

$$ST_x(t, f) = A \cdot e^{-j2\pi \cdot (f - f_0) \cdot t} \cdot (W(f_0, f))^* \tag{9}$$

Taking the partial derivative of both sides of Equation (9) with respect to t, we obtain:

$$\frac{\partial ST_x(t, f)}{\partial t} = A \cdot e^{-j2\pi \cdot (f - f_0) \cdot t} \cdot (W(f_0, f))^* \cdot (-j2\pi(f - f_0)) \tag{10}$$

By sorting out Equations (9) and (10), we can obtain:

$$\frac{\partial ST_x(t, f)}{\partial t} = j2\pi \cdot (f_0 - f) \cdot ST_x(t, f) \tag{11}$$

The frequency of the harmonic signal previously set can be expressed as $f_0 = f_0(t, f)$, and from Equation (11), we can obtain:

$$f_0(t, f) = f + (-\frac{j}{2\pi}) \cdot (ST_x(t, f))^{-1} \cdot \frac{\partial ST_x(t, f)}{\partial t} \tag{12}$$

When the signal is transformed by the *ST*, although the window width is designed to be adjustable and varies inversely with frequency, the signal energy concentration on the time-frequency line is still not high. To boost the time-frequency concentration and time-frequency resolution of the *ST*, it is necessary to remove the divergent energy outside the time-frequency line of the signal in the time-frequency distribution and retain the energy near the instantaneous frequency. For the signal containing noise in particular, to enhance the anti-noise characteristics of the signal, it is necessary to extract the time-frequency coefficient at the instantaneous frequency to generate a new spectrum.

Thus, the time-frequency coefficient at the instantaneous frequency of *ST* is extracted by virtue of the screening property of the δ function. According to the principle of the *SET* [18], the *SEST* model is constructed as:

$$SEST_x(t, f) = ST_x(t, f) \cdot \delta(f - f_0(t, f)) \tag{13}$$

where $\delta(f - f_0(t,f))$ is referred to as the synchronous extraction operator (*SEO*) of the *SEST*. According to Equation (13), the *SEST* can be regarded as further processing of the original *ST*. In light of Equations (12) and (13), the expression of $SEO(t,f)$ can be concluded as [31]:

$$SEO(t,f) = \delta(f - f_0(t,f)) = \delta(\frac{j}{2\pi} \cdot \frac{1}{ST_x(t,f)} \cdot \frac{\partial ST_x(t,f)}{\partial t}) \tag{14}$$

where $\frac{\partial ST_x(t,f)}{\partial t}$ is discretized by the finite-difference method, and we can obtain:

$$\frac{\partial ST_x(t,f)}{\partial t} = \frac{ST_x((t+\Delta t),f) - ST_x(t,f)}{\Delta t} \tag{15}$$

The *SEO* can be calculated by the following equation according to the definition of the δ function:

$$SEO(t,f) = \begin{cases} 1 & f = f_0(t,f) \\ 0 & f \neq f_0(t,f) \end{cases} \tag{16}$$

Taking the calculation error into consideration in practical applications, Equation (16) can be rewritten as:

$$SEO(t,f) = \begin{cases} 1 & \mathrm{Re}\left|\frac{j}{2\pi} \cdot \frac{1}{ST_x(t,f)} \cdot \frac{\partial ST_x(t,f)}{\partial t}\right| \prec \frac{\Delta f}{2} \\ 0 & \mathrm{Re}\left|\frac{j}{2\pi} \cdot \frac{1}{ST_x}(t,f) \cdot \frac{\partial ST_x(t,f)}{\partial t}\right| \geq \frac{\Delta f}{2} \end{cases} \tag{17}$$

where $\mathrm{Re}(\cdot)$ represents the real-part operation and $\Delta f = f_i - f_{i-1}$ represents the frequency sampling interval of the signal. Below is the algorithm flow chart of the harmonic signal *SEST* shown in Figure 1.

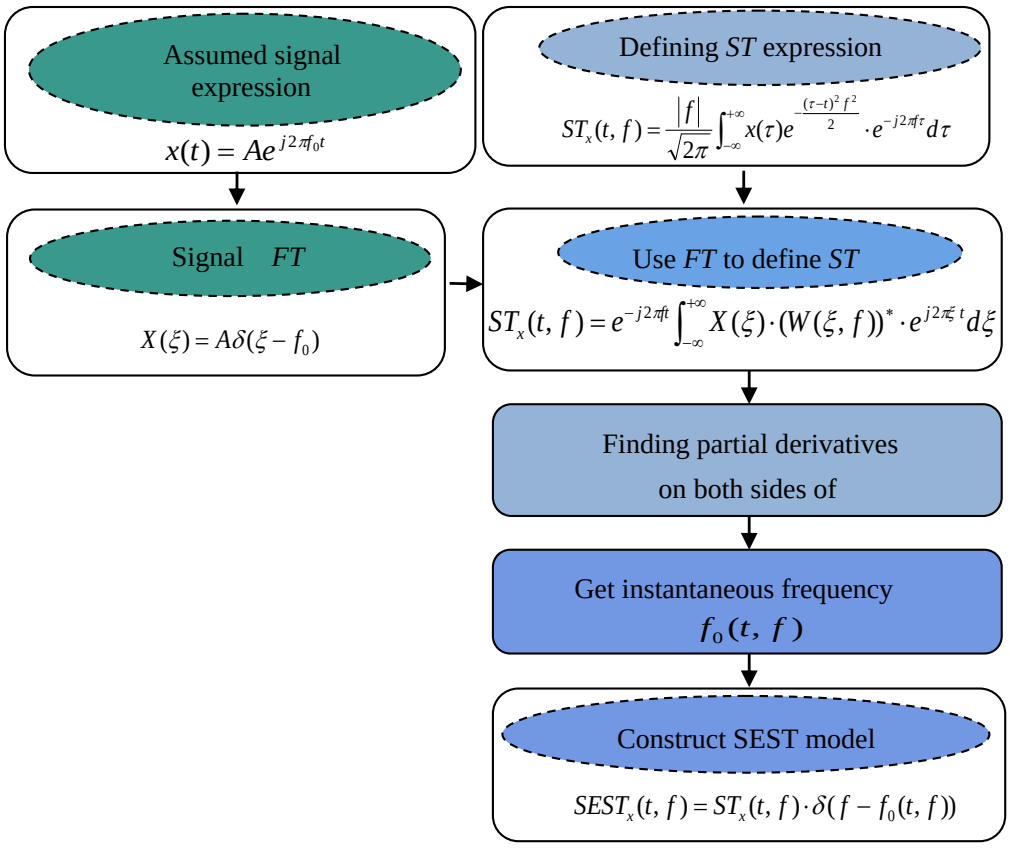

Figure 1. Algorithm flow chart of harmonic signal SEST.

2.2. Algorithm Implementation

All the simulation experiments in this paper were completed on the MATLAB R2018b platform.

All simulation comparisons in this paper were completed based on the following conditions. The Gaussian window width of *STFT* is set to 51; the Gaussian window width amplitude parameter of *GST* is set to 1 and the frequency adjustment parameter is set to 0.94; the localized Gaussian window width factor of *ST* is set to 1; the sifting stopping parameter of empirical mode decomposition in *HHT* is set to threshold is 0.05, threshold2 is 0.5, and tolerance is 0.05; for the Morlet wavelet basis function of *WT*, the bandwidth parameter is set to 5 and the center frequency parameter is set to 4; the Gaussian window width of *SET* is set to 1/8 of the number of signal rows; the Morlet wavelet basis function is used in *SWT*, and the frequency resolution in the output time-frequency representation is set to 0.05 Hz; *SEO* is extracted in *SEST* on the condition that the function value of *ST* is greater than 0.1 times the signal mean value.

The parameters of the noiseless harmonic signal $x(t) = A \cdot \cos(2\pi \cdot f_0 \cdot t)$ are listed in Table 1. An analysis of the *SEST* process of the harmonic signal is shown in the figure below.

Table 1. Parameters of the harmonic signal.

Parameters	Names	Values
A	amplitude	1
f_0	initial frequency	20 Hz
T	time width	1 s
f_s	sampling frequency	1000 Hz

The initial frequency of the harmonic signal is set as 20 Hz. As shown in Figure 2, the frequency of the harmonic signal does not change with time, and it belongs to the fundamental signal.

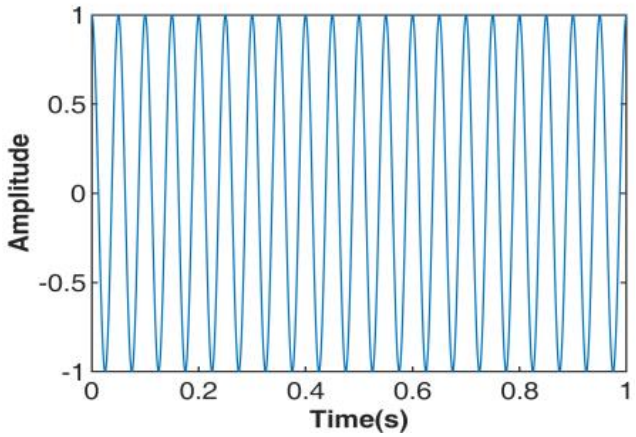

Figure 2. Time domain representation of harmonic signal.

Figure 3b shows that the time-frequency spectrum of the *ST* is the projection of Figure 3a on the xoy plane, which shows that the time-frequency ridge line of *ST* is wide and that the time-frequency energy diverges. Figure 3c shows the time-frequency energy divergence range of the *ST*; the half-peak width is 6 Hz, and the divergent energy will seriously affect the extraction of signal characteristics.

Figure 4b shows that the time-frequency spectrum of the *SEST* is the projection of Figure 4a on the xoy plane, which shows that the divergent energy outside the time-frequency ridge is eliminated after passing the *SEST* of the signal, the energy at the time-frequency ridge near 20 Hz is extracted, and the obtained time-frequency line is closer to the ideal time-frequency line. Figure 4c reveals the time-frequency energy concentration

range of the *SEST*; the half-peak width is 1 Hz, and the signal characteristics are effectively extracted. By contrasting Figure 3 with Figure 4, through the *SEST*, it is obvious that the time-frequency energy spectrum is clear and that there is no effect on the signal amplitude.

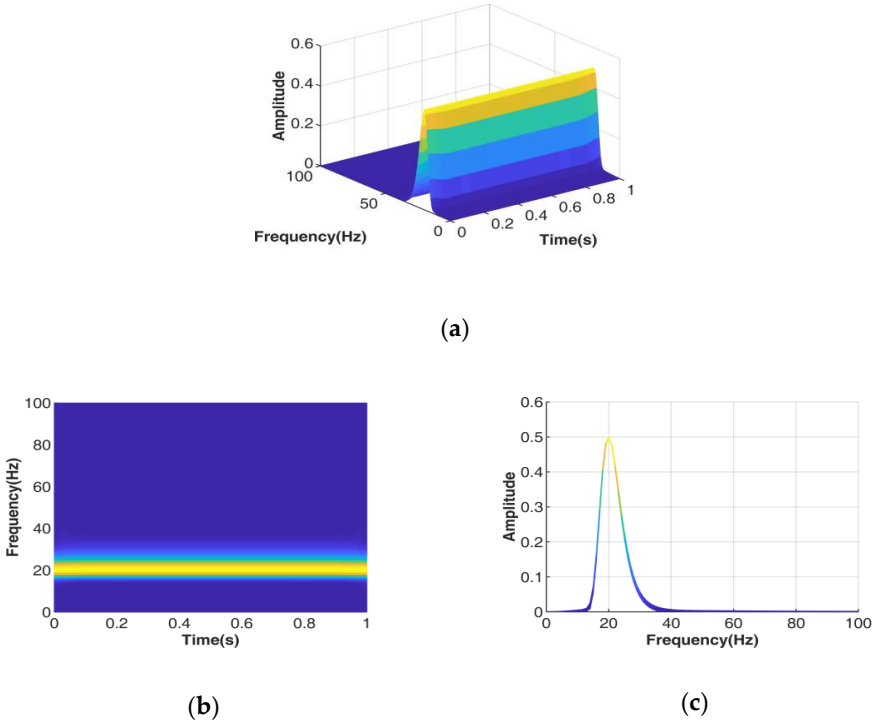

Figure 3. Time-frequency analysis of harmonic signal ST. (**a**) *ST* three-dimensional representation; (**b**) *ST* time-frequency representation; (**c**) *ST* frequency spectrum.

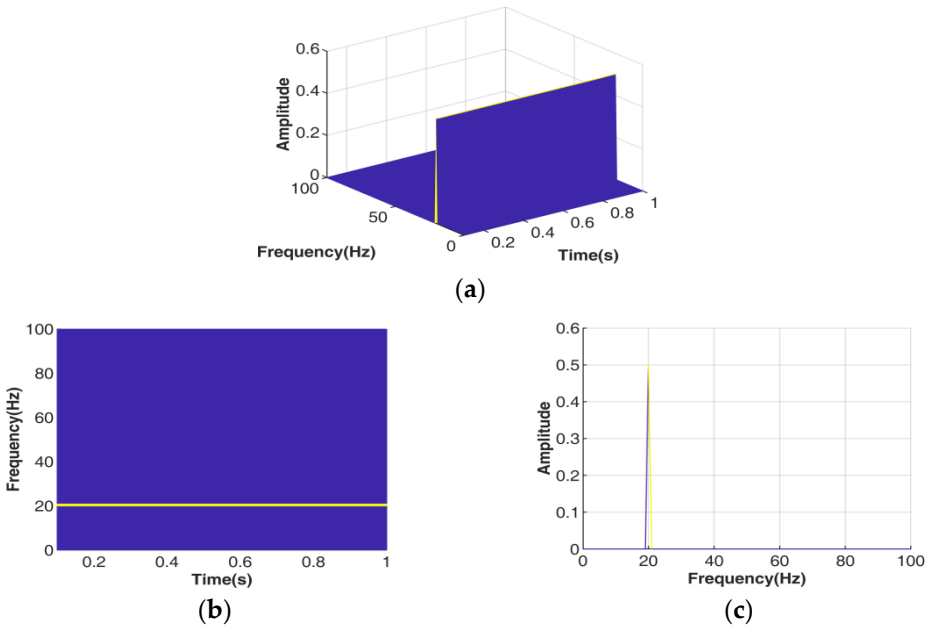

Figure 4. Time-frequency analysis of harmonic signal *SEST* process. (**a**) *SEST* three-dimensional representation; (**b**) *SEST* time-frequency representation; (**c**) *SEST* frequency spectrum.

3. Comparative Analysis with Other Transforms

According to the non-stationary rotor vibration, a multi-component signal model is constructed, and the proposed method in this paper is compared with other time-

frequency analysis methods. The following ways of combining the characteristics of rotor vibration faults, assuming that the simulation signal $x(t)$ is composed of three components, sinusoidal signal component $x_1(t)$, frequency modulation (FM) signal component $x_2(t)$ and amplitude modulation and frequency modulation (AM-FM) signal component $x_3(t)$, can be carried out. Namely:

$$x(t) = x_1(t) + x_2(t) + x_3(t) \tag{18}$$

where

$$x_1(t) = A_1 \cdot \sin(2\pi \cdot f_{01} \cdot t) \tag{19}$$

$$x_2(t) = A_2 \cdot e^{j \cdot 2\pi \cdot (f_{02} \cdot t + \frac{1}{2} k_2 \cdot t^2)} \tag{20}$$

$$x_3(t) = A_3 \cdot e^{j \cdot 2\pi \cdot (f_{03} \cdot t + \frac{1}{2} k_3 \cdot t^2)},\ A_3 = e^{r \cdot t} \tag{21}$$

3.1. Comparative Analysis of Time-frequency Distribution

3.1.1. *SEST* Proposed in This Paper

Parameter settings are shown in Table 2. Without noise, the *SEST* process of rotor vibration fault signal $x(t)$ is shown in Figure 5.

Table 2. Parameters of the rotor vibration fault signal $x(t)$.

Parameters	Names	Values
A_1	sinusoidal signal amplitude	1
f_{01}	sinusoidal signal initial frequency	130 Hz
A_2	FM signal amplitude	1.5
f_{02}	FM signal initial frequency	60 Hz
k_2	FM signal frequency modulation rate	−50 Hz/s
r	AM amplitude of AM-FM signal	1.5
f_{03}	AM-FM signal initial frequency	280 Hz
k_3	AM-FM signal frequency modulation rate	50 Hz/s
T	time width	1 s
f_s	sampling frequency	1024 Hz
SNR	signal-to-noise ratio	22 dB

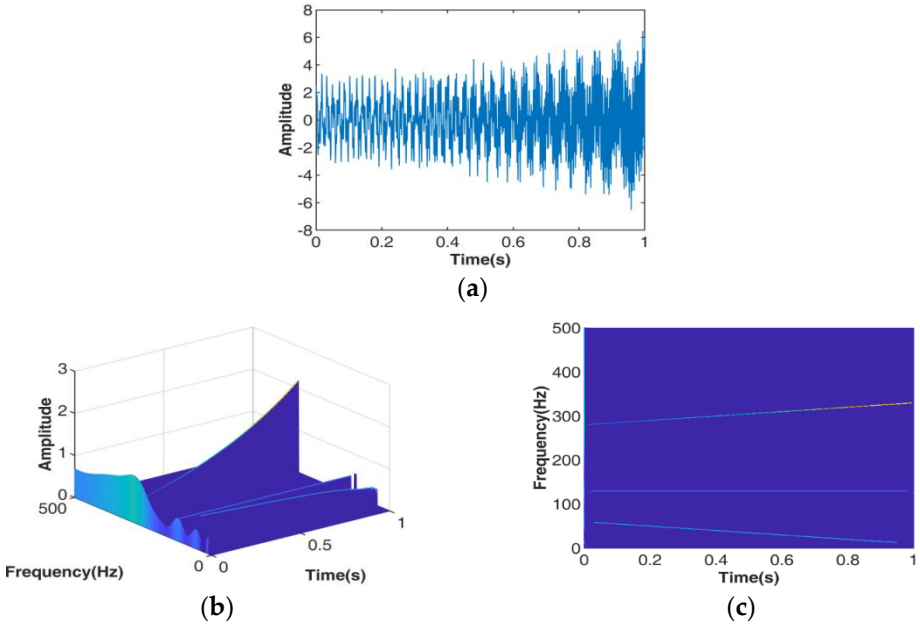

Figure 5. Time-frequency analysis of rotor vibration fault signal in *SEST*. (**a**) Signal time domain representation; (**b**) *SEST* three-dimensional representation; (**c**) *SEST* time-frequency representation.

It can be seen in the Figure 5 that the time-frequency concentration of the three signal components is good, and the time-frequency lines are clear straight lines, which can effectively extract the characteristics of the signals.

3.1.2. Comparative Analysis with Other Transforms

Parameter settings are shown in Table 2. Without noise, the time-frequency distribution of various transforms after normalization is shown in Figure 6.

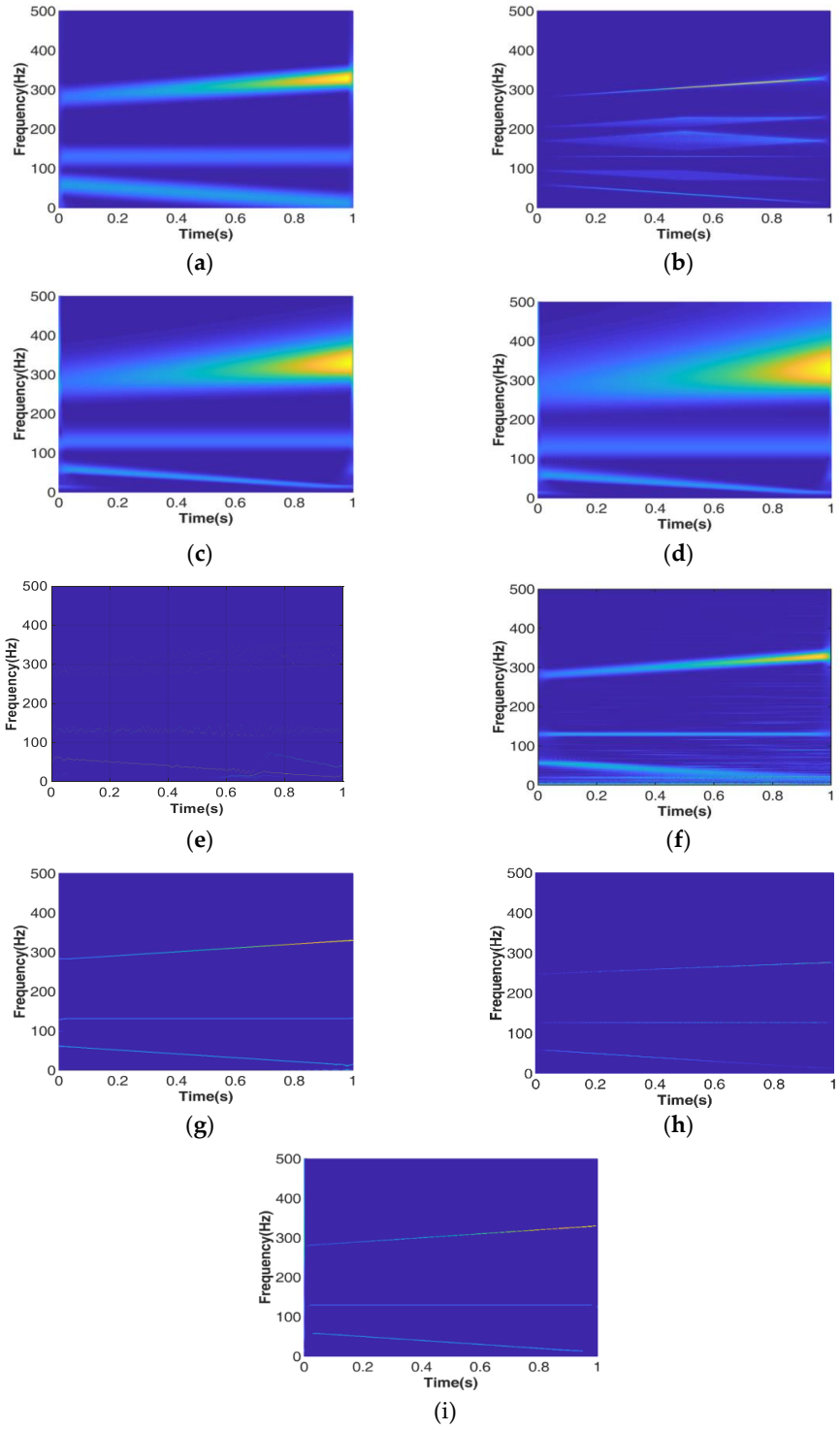

Figure 6. Comparison of various transform time-frequency representations of rotor vibration fault signals without noise. (**a**) *STFT*; (**b**) *WVD*; (**c**) *GST*; (**d**) *ST*; (**e**) *HHT*; (**f**) *WT*; (**g**) *SET*; (**h**) *SWT*; (**i**) *SEST*.

Figure 6a–i shows the time-frequency distributions of various transforms of the rotor vibration fault signal without noise interference. It can be seen in the figure that there is inter-component interference in *WVD*, and three component signals cannot be identified. The *STFT*, *GST*, *WT* and *ST* can identify three component signals, but the time-frequency energy divergence is more serious, especially the time-frequency energy of the FM signal component of the *STFT* and *WT*, and AM-FM signal components of the *ST* and *GST*, which diverge severely. The time-frequency spectrum of the *HHT* is slightly disordered and modal aliasing and false *IMF* components appear in the low-frequency band, but three component signals can be identified. *SET* can effectively extract the time-frequency ridge of three components, the time-frequency line is clear, and there is a little distortion at both ends of each time-frequency line. The *SWT* can also extract the time-frequency ridge of three components, but both ends of the time-frequency line are divergent; in particular, the extracted FM signal has weak time-frequency energy. The three component time-frequency lines of the *SEST* are clear straight lines, and the fuzzy energy at both ends of the time-frequency line is removed by using the screening characteristics of delta function. Compared with Figure 6g,i, the time-frequency ridge extracted in Figure 6i does not have distortion. From the performance of the time-frequency line, the time-frequency concentration of the *SEST* is better than that of other transforms, which indicates that the *SEST* can effectively extract the characteristics of multi-component signals and accurately identify rotor vibration fault signals.

3.2. Comparative Analysis of Time-Frequency Concentration

The components of the rotor vibration fault signal are transformed by the *STFT*, *WVD*, *GST*, *ST*, *HHT*, *WT*, *SET* and *SEST*, and the Rényi entropy is used to evaluate the time-frequency concentration of each transform [32]. Rényi entropy can extract the information from the time-frequency distribution without loss, so it is typically used as an index to objectively evaluate the time-frequency concentration.

Before the Rényi entropy is solved, the signal is first normalized according to the maximum and then solved using the following expression [33,34]:

$$H_\alpha(C) = \frac{1}{1-\alpha} \log_2 \frac{\iint |C(t,f)|^\alpha dtdf}{\iint |C(t,f)| dtdf} \tag{22}$$

where α is the order of the Rényi entropy and $C(t,f)$ is the time-frequency distribution.

In the experiment, the normalized third-order Rényi entropy criterion is used to evaluate the time-frequency concentration. The smaller the Rényi entropy is, the better the time-frequency concentration is.

3.2.1. Comparative Analysis without Noise Interference

Parameter settings are shown in Table 2. The results of Rényi entropy evaluation are as follows:

Table 3 shows that the Rényi entropy value of the *SEST* is the smallest, and its time-frequency concentration is good. The Rényi entropy value of *WVD* is the largest. The Rényi entropy values of the *WT*, *STFT*, *HHT*, *GST*, *ST* and *SET* decrease gradually, which indicates that the time-frequency concentration gradually improves.

Table 3. Rényi entropy evaluation results of rotor vibration fault signal.

Transform	Rényi Entropy Value	Transform	Rényi Entropy Value
STFT	1.3404	*ST*	1.1466
WVD	2.2789	*WT*	1.3952
GST	1.1476	*SET*	1.0033
HHT	1.3059	*SEST*	0.5246

3.2.2. Comparative Analysis with Noise Interference

Parameter settings are shown in Table 2. In the case of SNR = −5~+30 dB, the components of the rotor vibration fault signal are transformed by the *STFT*, *WVD*, *GST*, *ST*, *HHT*, *WT*, *SET* and *SEST*, and the Rényi entropy value results are shown in the following Figure 7.

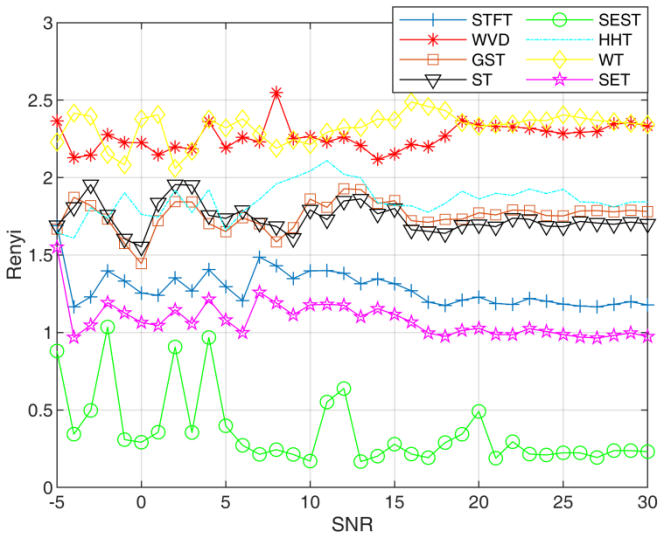

Figure 7. Rényi entropy evaluation results of rotor vibration fault signal with noise.

As shown in Figure 7, the time-frequency concentration of *SEST* proposed in this paper is excellent compared with other transforms in the case of SNR = −5~+30 dB.

3.3. Comparative Analysis of Algorithm Efficiency

The operating environment parameters are Windows10 and 64 bit operating system, Intel(R)Core(TM) i5-7200U CPU@2.50 GHz 2.71 GHz processor and 8.00 GB RAM. Parameter settings are shown in Table 2. The program was run 50 times; the running times of the algorithms are shown in Table 4.

Table 4. Algorithm run times.

Transform	Times/s	Transform	Times/s
STFT	1.371	*ST*	3.876
WVD	4.055	*WT*	4.594
GST	4.661	*SET*	8.188
HHT	1.538	*SEST*	6.615

As can be seen from Table 4, the operation time of *SEST* is longer than that of *ST*, but much shorter than that of *SET*. *SET* extracts the time-frequency ridge based on *STFT*. The value obtained by *SET* in the operation is complex matrix, so the speed of numerical operation is slow; *SEST* extracts the time-frequency ridge on the basis of *ST*. In the improvement of *SEST*, the *ST* result is transformed into [0, 1] matrix through *SEO*, and the data are binarized from high to low, so the subsequent processing speed is slightly faster. In the synchronous extraction phase, it takes 3.876 s to run the program 50 times, and when the *SEST* is constructed after *SET* binarization treatment, it takes 2.739 s to run the program 50 times. The *SEST* algorithm only takes 0.1323 s to run each time. After *STFT* operation, the value becomes a complex matrix. Then, *SET* is used to process the complex matrix, which takes a total of 8.188 s and takes a long time.

4. Time-Frequency Feature Extraction of Rotor Vibration Fault Signals

When the automobile is running, the vibration faults such as rotor imbalance, misalignment, bearing wear and loose gear meshing often occur. The vibration fault signal is usually composed of the fundamental component, first harmonic component, second harmonic component, 1/2 times harmonic component, AM/FM signal component and so on. When the unknown rotor vibration fault signal is transformed by *SEST*, its time-frequency line can be quickly extracted. The number of vibration fault signal components and the time-frequency variation of each component can be observed from the time-frequency diagram. Since the time-frequency lines of these vibration fault signal components are straight lines, so the Hough transform is used to detect the existence of the straight lines, and the straight lines detection problem in the time-frequency domain is transformed into the peaks search problem in the polar diameter and polar angle domain, and then the parameters such as the initial frequency and the frequency modulation rate of the signal components are estimated through the peak search.

The time-frequency characteristics of each signal component are extracted and compared with the time-frequency characteristics of the standard signal. At the same time, it is further matched with the common rotor vibration fault characteristics so the rotor vibration fault can be identified.

4.1. Rotor Misalignment Vibration

When the bearing of the motor is worn seriously over a long time, it can easily cause vibration faults from rotor misalignment. The vibration fault signal is mainly composed of three frequency components, namely, the fundamental component, second harmonic component and third harmonic component. The parameters are shown in Table 5. The simulation results are as follows.

Table 5. Parameters of the rotor misalignment vibration fault signal.

Parameters	Names	Values
A_1	fundamental signal component amplitude	1
f_{01}	fundamental signal component frequency	24 Hz
T	time width	1 s
f_s	sampling frequency	2048 Hz
SNR	signal-to-noise ratio	20 dB

It can be seen in Figure 8 that compared with Figure 8a, the signal waveform of the rotor in Figure 8c is distorted, and the vibration fault of the rotor is predicted. Comparing Figure 8d with Figure 8b, it can be seen that the time-frequency distribution of the three components is clearly shown in Figure 8d. In addition to the fundamental signal component, two harmonic signal components are identified, respectively, near 48 Hz and 75 Hz so that the rotor misalignment vibration fault can be diagnosed.

4.2. Rotor Unbalance Vibration

The unbalance vibration fault of an automobile rotor is a common fault form. Due to the errors in the manufacture and installation of the rotor: uneven heating, rotor wear, scaling and loose or falling parts during operation, it is easy to cause unbalanced vibration of the rotor. At a certain rotor speed, the amplitude often presents nonlinear vibration characteristics, and the vibration frequency spectrum is relatively rich. In addition to the fundamental frequency component, there are also high-frequency components. It is assumed that the rotor unbalance vibration signal $x(t)$ is composed of the fundamental component $x_1(t)$, second harmonic component $x_2(t)$, third harmonic component $x_3(t)$ and the AM-FM signal component $x_4(t)$. Namely:

$$x(t) = x_1(t) + x_2(t) + x_3(t) + x_4(t) \tag{23}$$

where

$$x_4(t) = A_4 \cdot e^{j \cdot 2\pi \cdot (f_{04} \cdot t + \frac{1}{2} k_4 \cdot t^2)}, \; A_4 = e^{r \cdot t} \tag{24}$$

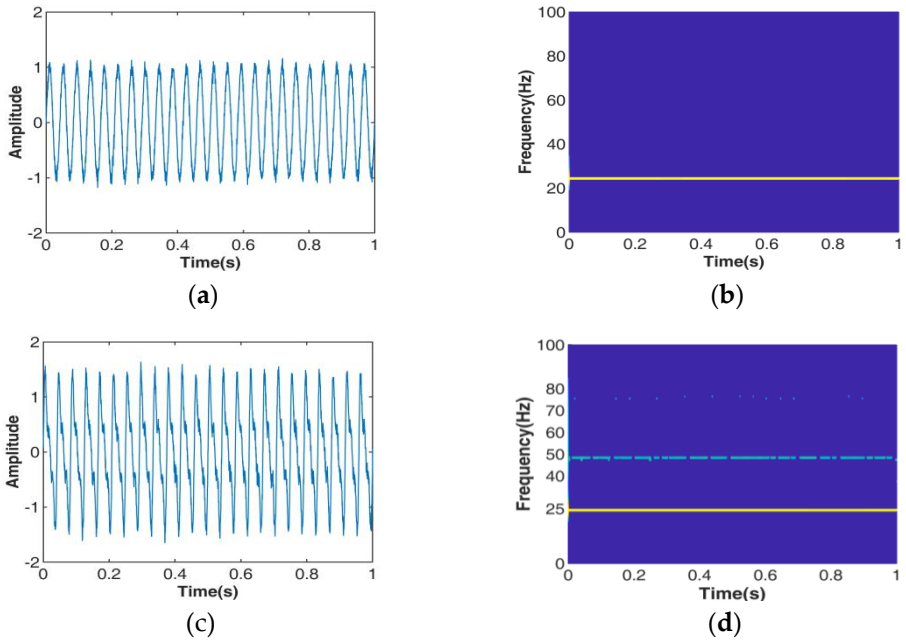

Figure 8. Comparison of rotor in both normal and misalignment vibration states. (**a**) Time domain representation of rotor in normal state; (**b**) *SEST* time-frequency representation of rotor in normal state; (**c**) time domain representation of rotor misalignment vibration; (**d**) *SEST* time-frequency representation of rotor misalignment vibration.

The parameters are shown in Table 6.

Table 6. Parameters of the rotor unbalance vibration fault signal.

Parameters	Names	Values
A_1	fundamental signal component amplitude	1
f_{01}	fundamental signal component frequency	20 Hz
r	AM amplitude of AM-FM signal component	1.5
f_{04}	AM-FM signal component initial frequency	64 Hz
k_4	AM-FM signal component frequency modulation rate	31 Hz/s
T	time width	1 s
f_s	sampling frequency	2048 Hz
SNR	signal-to-noise ratio	20 dB

The simulation results are as follows.

It can be seen in Figure 9 that compared with Figure 9a, the frequency and the amplitude of the rotor signal in Figure 9c have changed, indicating that the rotor appears to have vibration faults. Comparing Figure 9d with Figure 9b, it can be found that the time-frequency distribution of four signal components is shown in Figure 9d. In addition to the fundamental component, the second harmonic signal component can be clearly identified at 40 Hz, the third harmonic signal component is identified near 53–60 Hz, and the FM signal component is identified between 64 and 95 Hz. Figure 9e clearly shows the existence of four signal components and the change of signal amplitude; it especially clearly shows that the amplitude of FM signal is increasing, which belongs to the AM-FM signal. As a result, the type of rotor vibration can be quickly and accurately identified based on *SEST*, and the frequency source of the fault signal can be diagnosed.

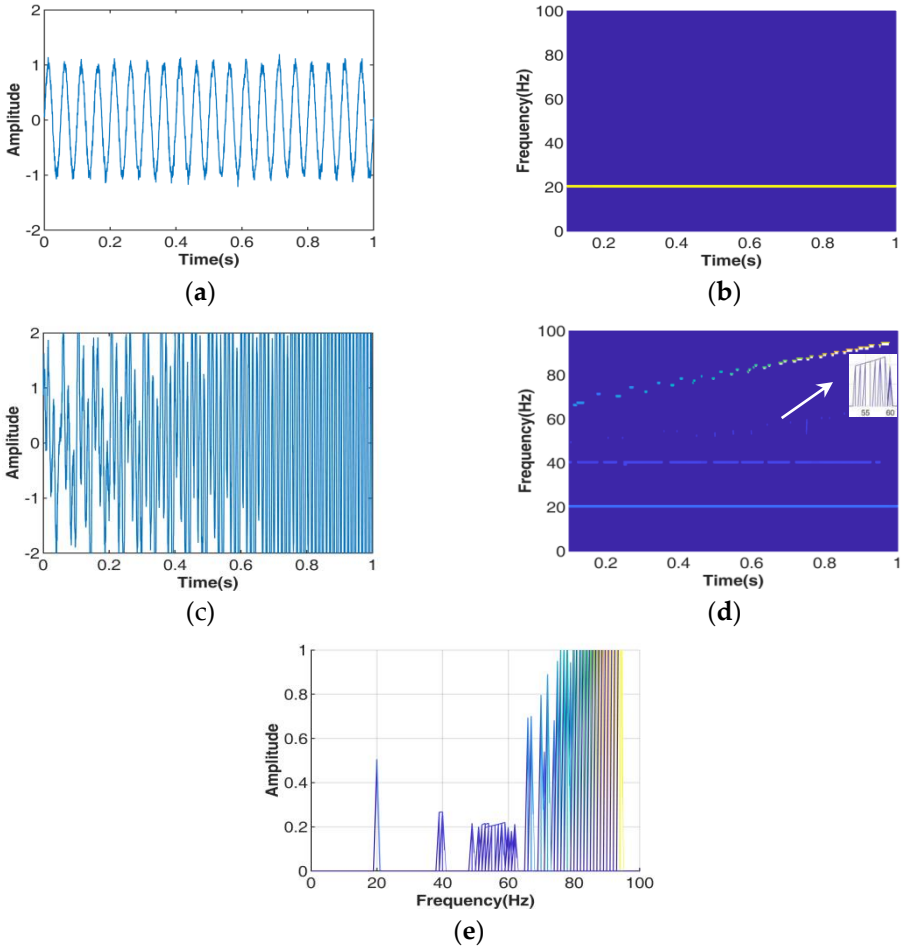

Figure 9. Comparison of rotor in both normal and unbalanced vibration states. (**a**) Time domain representation of rotor in normal state; (**b**) *SEST* time-frequency representation of rotor in normal state; (**c**) time domain representation of rotor unbalance vibration; (**d**) *SEST* time-frequency representation of rotor unbalance vibration; (**e**) *SEST* frequency spectrum of rotor unbalance vibration.

4.3. Rotor Bearing Wear Vibration

When the rotor bearing is slightly worn, it shows 1/2 times and 1/3 times harmonic vibration components. In the later stage of wear, the vibration spectrum presents 1 times frequency components, accompanied by slightly higher harmonic components. It is assumed that the rotor bearing wear vibration signal is composed of the 1/2 times and 1/3 times harmonic vibration components, fundamental components, and second harmonic and third harmonic components. The parameters are shown in Table 7.

Table 7. Parameters of the rotor bearing wear vibration fault signal.

Parameters	Names	Values
A_1	fundamental signal component amplitude	1
f_{01}	fundamental signal component frequency	30 Hz
T	time width	1 s
f_s	sampling frequency	2048 Hz
SNR	signal-to-noise ratio	20 dB

The simulation results are as follows.

It can be seen in Figure 10 that compared with Figure 10a, the frequency and amplitude of the rotor signal have changed in Figure 10c, indicating that the rotor has a vibration fault. Comparing Figure 10d with Figure 10b, it can be seen that the time-frequency distribution

of five signal components is shown in Figure 10d. In addition to the fundamental component, the 1/3 times harmonic component is clearly identified at 10 Hz and the second harmonic component is identified near 60 Hz. The third harmonic component is identified between 93 Hz and 95 Hz, which deviates from the preset value by about 5 Hz and the signal amplitude is weak. At the position of 11–16 Hz, another frequency division harmonic component appears, which is interrupted by the interference of 1/3 times harmonic component. From these, it can be seen that the *SEST* can quickly identify the components of rotor vibration signal and predict the type of rotor vibration.

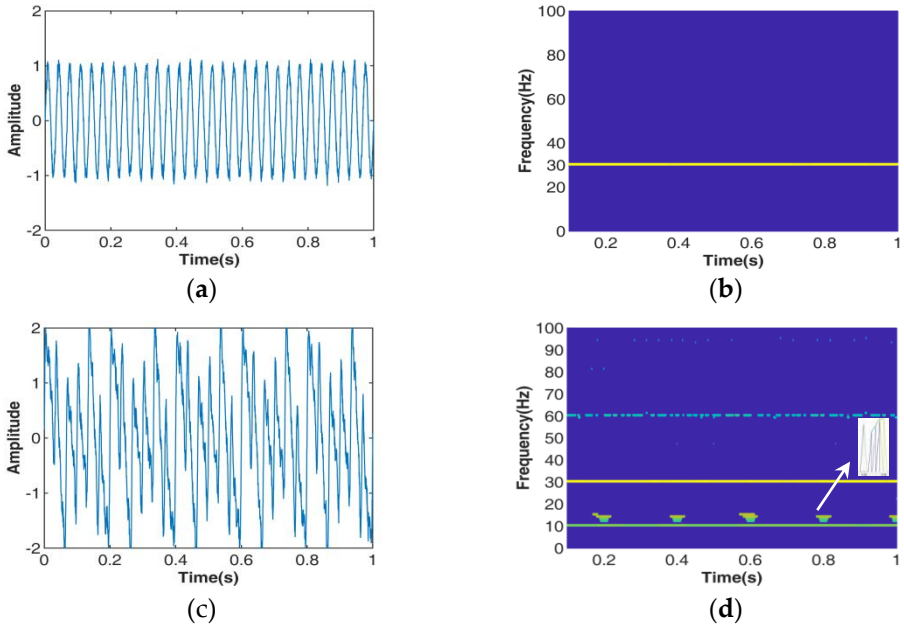

Figure 10. Comparison of rotor in both normal and bearing wear vibration states. (**a**) Time domain representation of rotor in normal state; (**b**) *SEST* time-frequency representation of rotor in normal state; (**c**) time domain representation of rotor bearing wear vibration; (**d**) *SEST* time-frequency representation of rotor bearing wear vibration.

5. Conclusions

In this paper, a vibration fault signal identification method via *SEST* is proposed and the *SEST* model is constructed. In order to verify the effectiveness of the proposed method, the proposed *SEST* method is compared with the existing time-frequency analysis methods. According to the time-frequency representation diagram and Rényi entropy, compared with other methods, it shows that *SEST* has high time-frequency concentration and strong noise resistance. At the same time, the vibration faults such as rotor misalignment, rotor imbalance and bearing wear are used to further verify the effectiveness of the *SEST* proposed in this paper.

The *SEST* proposed in this paper is suitable for fault signal detection of machinery and automobile, as well as signal processing in the fields of electronic countermeasure, artificial intelligence and so on. In automobile application, the vibration fault signal of automobile rotor diagnosed and identified is transmitted to the on-board intelligent system in real-time, so as to facilitate the timely planning of the emergency driving route through internet of vehicles and provide services for the realization of intelligent transportation. At the same time, it is more conducive to the realization of automatic driving under the background of vehicle and road cooperation and the rapid construction of smart cities based on the internet of things.

Supplementary Materials: The following supporting information can be downloaded at: https://www.mdpi.com/article/10.3390/electronics11091300/s1.

Author Contributions: Methodology, X.L. (Xuemei Li) and C.W.; software, X.L. (Xuelian Liu); validation, B.X. and Z.W. All authors have read and agreed to the published version of the manuscript.

Funding: This research was funded by the science and technology research project of the education department of Jilin Province, China, grant number 49710 JJKH20220014KJ and the science and technology development plan project of Baicheng city of Jilin Province, China.

Institutional Review Board Statement: Not applicable.

Informed Consent Statement: Not applicable.

Data Availability Statement: The data presented in this study are available in Supplementary Materials.

Acknowledgments: The manuscript was supported by the Department of Science and Technology of Jilin Province (Grant No.20190302089GX) and Jilin Province Advanced Control Technology and Intelligent Automation Equipment Lab and intelligent perception and control research center of Baicheng Normal University.

Conflicts of Interest: The authors declare no conflict of interest.

References

1. Xin, P.; Ge, B.; Tao, D.; Lv, P. Electromagnetic torque characteristics analysis of nuclear half-speed turbine generator with stator winding inter-turn short circuit fault. *Electr. Eng. Technol.* **2021**, *16*, 2055–2063. [CrossRef]
2. Liu, Y.; Zhao, Y.; Li, J.; Lu, H.; Ma, H. Feature extraction method based on nofrfs and its application in faulty rotor system with slight misalignment. *Nonlinear Dyn.* **2020**, *99*, 1763–1777. [CrossRef]
3. Maheswari, R.U.; Umamaheswari, R. Trends in non-stationary signal processing techniques applied to vibration analysis of wind turbine drive train-a contemporary survey. *Mech. Syst. Signal Process.* **2017**, *85*, 296–311. [CrossRef]
4. Varanis, M.; Silva, A.L.; Balthazar, J.M.; Pederiva, R. A tutorial review on time-frequency analysis of non-stationary vibration signals with nonlinear dynamics applications. *Braz. J. Phys.* **2021**, *51*, 859–877. [CrossRef]
5. Żak, G.; Wyłomańska, A.; Zimroz, R. Local damage detection method based on distribution distances applied to time-frequency map of vibration signal. *IEEE Trans. Ind. Appl.* **2018**, *54*, 4091–4103. [CrossRef]
6. Verma, N.K.; Gupta, R.; Sevakula, R.K. Signal transforms for feature extraction from vibration signal for air compressor monitoring. In Proceedings of the Tencon IEEE Region 10 Conference, Bangkok, Thailand, 22–25 October 2014.
7. Narasimhan, S.; Nagarajaiah, S. A STFT semiactive controller for base isolated buildings with variable stiffness isolation systems. *Eng. Struct.* **2005**, *27*, 514–523. [CrossRef]
8. Huang, M.; Zhu, L.; Zhang, Z.; Han, J.; Liu, B. Fault vibration signal analysis of air vehicle flying based on STFT. *Equip. Environ. Eng.* **2021**, *18*, 62–65.
9. Liu, J.; Li, X.; Qiao, X.; Li, H. Time-frequency analysis of vibration signal from cylinder head of a diesel engine based on EMD and STFT. *Noise Vib. Control* **2013**, *33*, 133–137.
10. Wang, Y.; Zheng, L.; Gao, Y.; Li, S. Vibration signal extraction based on FFT and least square method. *IEEE Access* **2020**, *8*, 224092–224107. [CrossRef]
11. Mao, Y.; Fang, S.; Li, T.; Ma, H. Study on the vibration characteristic of turbine rotor eccentricity based on FFT. In Proceedings of the 7th International Conference on Mechanical and Aerospace Engineering, London, UK, 18–22 July 2016.
12. Le, Y.; Li, H.; You, C.; Hu, X.; Liu, D.; Xiao, Z. On the Feature Extraction Method for Rotor Vibration Signal based on FFT and EWT. *Hydropower New Energy* **2019**, *33*, 34–38+65.
13. Liu, J.; Yao, J.; Liu, X. Generalized S transform with adaptive optimized window and its application in seismic signal analysis. *Inf. Technol. J.* **2013**, *12*, 276–286. [CrossRef]
14. Chen, H.; Yi, Y.; Chen, W.; Chen, P.; Shen, J. Fault Diagnosis Method of Gearbox Bearings Based on Generalized S-transform. *China Mech. Eng.* **2017**, *28*, 51–56.
15. Hu, Y.; Tu, X.; Li, F. High-order synchrosqueezing wavelet transform and application to planetary gearbox fault diagnosis. *Mech. Syst. Signal Process.* **2019**, *131*, 126–151. [CrossRef]
16. Chen, X.; Cheng, G.; Shan, X.; Hu, X.; Guo, Q.; Liu, H. Research of weak fault feature information extraction of planetary gear based on ensemble empirical mode decomposition and adaptive stochastic resonance. *Measurement* **2015**, *73*, 55–67. [CrossRef]
17. Yu, G. Research on Excavator Vibration and Sound Signal Processing Using Time-Frequency Analysis Method and Implementation. Ph.D. thesis, Shandong University, Ji'nan, China, 2016.
18. Yu, G.; Yu, M.; Xu, C. Synchroextracting transform. *IEEE Trans. Ind. Electron.* **2017**, *64*, 8042–8054. [CrossRef]
19. Yu, Z.; Yu, C.; Chen, X.; Huang, T. Adaptive multiple second-order synchrosqueezing wavelet transform and its application in wind turbine gearbox fault diagnosis. *Meas. Sci. Technol.* **2022**, *33*, 15110. [CrossRef]

20. Liu, Y.; Li, K.; Chen, P. Fault diagnosis for rolling bearings based on synchrosqueezing wavelet transform. *China Mech. Eng.* **2018**, *29*, 585–590.
21. Welch, P. The Use of Fast Fourier Transform for the Estimation of Power Spectra: A Method Based on Time Averaging over Short, Modified Periodograms. *IEEE Trans. Audio Electroacoust.* **1967**, *15*, 70–73. [CrossRef]
22. Schmidt, R. Multiple Emitter Location and Signal Parameter Estimation. *IEEE Trans. Antennas Propag.* **1986**, *34*, 276–280. [CrossRef]
23. Xu, B.; Tian, S. Detection for Broken Rotor Fault in Induction Motors Combining Multiple Signal Classification Algorithm with Extended Prony. *J. North China Electr. Power Univ.* **2015**, *42*, 16–23.
24. Dehina, W.; Boumehraz, M.; Kratz, F. Detect ability of rotor failure for induction motors through stator current based on advanced signal processing approaches. *Int. J. Dyn. Contorl* **2021**, *9*, 1–15.
25. Roy, R.; Paulraj, A.; Kailath, T. Estimation of Signal Parameters via Rotational Invariance Techniques-ESPRIT. *IEEE Trans. Acoust. Speech Signal Processing* **1987**, *67*, 341–350.
26. Capon, J. High-Resolution frequency-Wavenumber Spectrum Analysis. *Proc. IEEE* **1969**, *57*, 1408–1418. [CrossRef]
27. Stoica, P.; Li, J.; Ling, J. Missing Data Recovery Via a Nonparametric Iterative Adaptive Approach. *Signal Process. Lett.* **2009**, *4*, 241–244. [CrossRef]
28. Lei, L.; Zhou, J. Parameter estimation in multi-antenna system based on iterative adaptive approach. *Matec Web Conf.* **2018**, *232*, 4064. [CrossRef]
29. Guan, J. Missing Data Recovery of Frequency Hopping Signal Based on Iterative Adaptive Approach. *Telecommun. Eng.* **2020**, *60*, 791–797.
30. Chen, H.; Kang, J.; Chen, Y.; Xu, D.; Hu, Y. An improved time-frequency analysis method for hydrocarbon detection based on EWT and SET. *Energies* **2017**, *10*, 1090. [CrossRef]
31. Yu, G.; Wang, Z.; Zhao, P.; Li, Z. Local maximum synchrosqueezing transform: An energy-concentrated time-frequency analysis tool. *Mech. Syst. Signal Process.* **2019**, *117*, 537–552. [CrossRef]
32. GLeite, N.P.; Araújo, A.M.; Rosas, P.A.C.; Stosic, T.; Stosic, B. Entropy measures for early detection of bearing faults. *Phys. A Stat. Mech. Its Appl.* **2019**, *514*, 458–472.
33. Baraniuk, R.G.; Flandrin, P.; Janssen, A.J.E.M.; Michel, O.J.J. Measuring time-frequency information content using the Rényi entropies. *IEEE Trans. Inf. Theory* **2001**, *47*, 1391–1409. [CrossRef]
34. He, D.; Cao, H.; Wang, S.; Chen, X. Time-reassigned synchrosqueezing transform: The algorithm and its applications in mechanical signal processing. *Mech. Syst. Signal Processing* **2019**, *117*, 255–279. [CrossRef]